

# Multiple steady states in exchange flows across faults and the dissolution of CO<sub>2</sub>

Andrew W. Woods<sup>1,†</sup>, Marc Hesse<sup>2</sup>, Rachel Berkowitz<sup>1</sup> and  
Kyung Won Chang<sup>2</sup>

<sup>1</sup>BP Institute, University of Cambridge, Madingley Road, Cambridge CB3 0EZ, UK

<sup>2</sup>Department of Geological Sciences, University of Texas, Austin, TX 78712, USA

(Received 25 March 2014; revised 8 January 2015; accepted 8 February 2015;  
first published online 16 March 2015)

We develop a model of the steady exchange flows which may develop between two aquifers at different levels in the geological strata and across which there is an unstable density stratification, as a result of their connection through a series of fractures. We show that in general there are multiple steady exchange flows which can develop, depending on the initial conditions, and which may involve a net upwards or downwards volume flux. We also show that there is a family of equilibrium exchange flows with zero net volume flux, each characterised by a different interlayer flux of buoyancy. We present experiments which confirm our simplified model of the exchange flow. Such exchange flows may supply unsaturated water from a deep aquifer to drive dissolution of a structurally trapped pool of geologically stored CO<sub>2</sub>, once the water in the aquifer containing the trapped pool of CO<sub>2</sub> has become saturated in CO<sub>2</sub>, and hence relatively dense. Such exchange flows may also lead to cross-contamination of aquifer fluids, which may be of relevance in assessing risks of geological storage systems.

**Key words:** convection, porous media

## 1. Introduction

The geological sequestration of large volumes of CO<sub>2</sub> into subsurface aquifers and depleted oil and gas fields has been advocated by the IPCC (2005) as a means of reducing atmospheric emissions of CO<sub>2</sub>. A key challenge for this technology concerns the modelling of the long-term fate of the CO<sub>2</sub>. Following injection into the subsurface, one may envisage that a plume of CO<sub>2</sub> develops and migrates upwards until reaching a structural trap where it may accumulate (Pruess *et al.* 2003; Hesse, Tchelpi & Orr 2008), although some of the CO<sub>2</sub> may dissolve into the groundwater (Lindeberg & Wessel-Berg 1997; Riaz *et al.* 2006; Ennis-King & Paterson 2007; Pau *et al.* 2009) or become capillary trapped (Bennion & Bachu 2008; Hesse *et al.* 2008; Farcas & Woods 2009; Woods 2015) en route to the trap. The CO<sub>2</sub> which accumulates in a structural trap may then gradually dissolve into the underlying groundwater; this represents an important step in the long-term stability of the sequestered CO<sub>2</sub>, and has

† Email address for correspondence: [andy@bpi.cam.ac.uk](mailto:andy@bpi.cam.ac.uk)

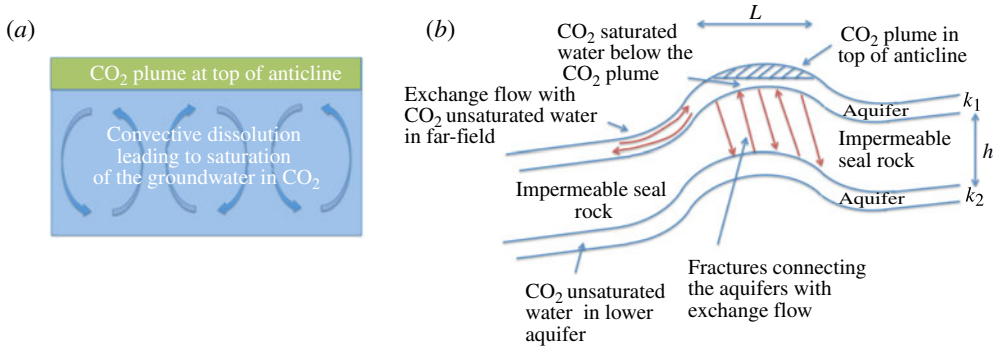


FIGURE 1. (Colour online) (a) An illustration of the convective dissolution within the upper aquifer, which leads to CO<sub>2</sub> saturation of the formation fluid in the upper aquifer. (b) An illustration of the larger-scale flow domain showing the anticline or fold which traps the CO<sub>2</sub> plume in the upper aquifer. Also shown are the fractures connecting the upper and lower aquifers. The greater density of the CO<sub>2</sub>-saturated formation water, coupled with any pressure difference between the aquifers, relative to the hydrostatic pressure difference, leads to possible counterflow and hence supply of undersaturated fluid to the upper aquifer.

attracted much scientific investigation (Pruess *et al.* 2003; Riaz *et al.* 2006; Hewitt, Neufeld & Lister 2013). Since the CO<sub>2</sub>-saturated water is relatively dense, convective flows can develop, with unsaturated water rising towards the CO<sub>2</sub> interface, replacing the dense CO<sub>2</sub>-saturated water, thereby promoting convective dissolution. Various models have been developed to quantify the flux associated with such convective dissolution since it may be one of the key rate-limiting steps. As one end-member, the dissolution may develop in a deep, permeable layer in which a convective mixing flow develops (figure 1) (Riaz *et al.* 2006). The CO<sub>2</sub>-saturated and unsaturated water then mix until the whole depth of the water in the aquifer below the CO<sub>2</sub> pool has become saturated in CO<sub>2</sub> and the convection shuts off (Hewitt *et al.* 2013). Analyses have been carried out to explore the role of heterogeneity and background flows in such convective dissolution (Kuznetsov & Nield 2011, 2012; Ranganathan *et al.* 2012). As an idealised limit, in an isotropic formation of effective permeability  $k$  and with a density contrast between unsaturated groundwater and CO<sub>2</sub>-saturated groundwater,  $\Delta\rho$ , plumes typically descend with Darcy velocity

$$u = \frac{k\Delta\rho g}{\mu}, \quad (1.1)$$

where  $\mu$  is viscosity and  $g$  acceleration due to gravity, and this may have value of order  $10^{-8}$ – $10^{-9}$  m s<sup>-1</sup>. We infer that provided there is a source of unsaturated water, then with CO<sub>2</sub> concentration of 1–3 wt% following dissolution into the water, the trapped plume of CO<sub>2</sub> may dissolve into the underlying fluid at a rate determined by the speed of convective plumes times this solubility, leading to an estimate of 100–1000 kg CO<sub>2</sub> m<sup>-2</sup> per thousand years. Trapped pockets of CO<sub>2</sub> may therefore dissolve over thousands of years (Riaz *et al.* 2006; Woods & Espie 2012).

Once the fluid below the structural trap has become saturated in CO<sub>2</sub>, unsaturated water from more distal locations is required to continue the dissolution process. If the aquifer is of limited vertical extent, but has a shallow inclination, then a

convective exchange flow may develop between the unsaturated water in the laterally distant parts of the aquifer and the CO<sub>2</sub>-saturated water below the structural trap, providing a source of fresh water for the dissolution (figure 1) (Woods & Espie 2012). Owing to the very small speed, the near-horizontal current of unsaturated water migrating towards the structurally trapped plume of CO<sub>2</sub> may require tens to hundreds of thousands of years to dissolve the CO<sub>2</sub>, and eventually the flow may become controlled by shear-dispersion (Szulczewski, Hesse & Juanes 2014).

Although the above models provide end-members for the rate of convection-driven dissolution, they are based on a picture of a single reservoir within an impermeable country rock. Many sedimentary rocks are composed of a series of laterally extensive and relatively thin layers, with shale barriers or more extensive layers of siltstone which restrict cross-layer flow. One may therefore envisage a third scenario in which there are stacked sedimentary layers, each tens of metres thick and separated by nearly impermeable siltstone or shale layers, ranging from metres to tens of metres in thickness, forming a highly layered system (Phillips 1991). The seal rock may become fractured following emplacement owing to compaction, folding or other tectonic processes. Such fractures may then provide a pathway between neighbouring aquifers, and hence a source of additional unsaturated water which may enhance the CO<sub>2</sub> dissolution process (figure 1*b*).

The purpose of this work is to explore the vertical convective exchange associated with such fractures between two aquifers. In the context of CO<sub>2</sub> sequestration, relatively dense CO<sub>2</sub>-saturated brine would form directly below a CO<sub>2</sub> plume as a result of convective dissolution (e.g. Lindeberg & Wessel-Berg 1997; Ennis-King & Paterson 2007). If there is a deeper aquifer which contains less-dense brine, undersaturated in CO<sub>2</sub>, then ultimately, following the injection phase, this may develop a convective exchange flow along the fractures with the CO<sub>2</sub>-saturated water. We note that during the CO<sub>2</sub> injection phase, the system is likely to be overpressured, and any fractures may initially be filled with the CO<sub>2</sub>-saturated brine from the upper aquifer. However, following the end of the injection phase, as the system decompresses, and the flows become dominated by buoyancy forces, then an upward rising localised plume may develop in one or more fractures, owing to the buoyancy of the lower aquifer fluid relative to the CO<sub>2</sub>-saturated fluid in the upper aquifer. Such plumes lead to an exchange of fluid in the fracture, with the heavier CO<sub>2</sub>-saturated brine in the fracture descending to the lower aquifer. As some of these plumes rise upwards in the fractures, one can envisage the development of a convective exchange between the two aquifers, as we have observed in our experiments (§ 3). The main focus of this paper is to describe the different patterns of steady convective flow which may develop in a multiply fractured seal layer after the transient development of the flow, which depends in detail on the initial conditions, although we also discuss the counterflow which may develop in a single, laterally extensive fracture (Tartakovsky & Meakin 2005; Chen & Zhang 2010).

Once an exchange flow is established, it may then supply CO<sub>2</sub>-undersaturated water to the upper aquifer leading to continuing dissolution of the CO<sub>2</sub>. By quantifying the flux, we can assess its magnitude and importance in dissolving the CO<sub>2</sub> plume relative to the lateral exchange flow which brings unsaturated water from laterally distant parts of the formation (figure 1*b*) (Woods & Espie 2012).

In our modelling, we assume that the density of the fluid in the upper aquifer is greater owing to the dissolution of CO<sub>2</sub> into the water in this aquifer. Provided this leads to the density of the fluid in this upper aquifer exceeding that in the lower aquifer then the convective exchange flow described herein can develop, even

if prior to the injection and dissolution of  $\text{CO}_2$ , the fluid in the lower aquifer was initially denser than that in the upper aquifer owing for example to compositional differences. In this context, we note that there is a more general set of exchange flow processes which may lead to groundwater mixing in situations in which unstable buoyancy gradients develop (Flowers & Hunt 2007). Indeed, if two aquifers are initially isolated, and the fluid in the upper aquifer is of greater composition and hence density, then if a series of faults open up to connect the aquifers, for example following a tectonic event, exchange flows analogous to those discussed in this work may develop. However, it is also possible that the fluid in the lower aquifer is more dense, and in this case, the buoyancy forces tend to suppress convective exchange between the aquifers. In that case there may be some initial pressure-driven exchange flow, but as the pressure difference between the two aquifers decreases, such flows will become suppressed by the stabilising effect of buoyancy.

## 2. Model system

We model a system in which the geological strata includes an impermeable stratigraphic horizon of vertical extent  $h$  separating an upper and lower permeable layer. We envisage that there is a structural trap of  $\text{CO}_2$  and that owing to convective dissolution of the  $\text{CO}_2$ , the water directly below the  $\text{CO}_2$  plume is  $\text{CO}_2$  saturated with density  $\rho + \Delta\rho$ , while the formation water in the lower layer is unsaturated and has density  $\rho$  (figure 1). We also assume that the two permeable regions are connected by  $m$  parallel fractures, with permeability  $k_i$  and aperture of width  $d_i$ ,  $i = 1, \dots, m$ , located around the anticline structure.

We now show that depending on the pressure difference between the aquifers, this density contrast can drive a steady convective exchange flow through the fractures. To illustrate the phenomenon, we assume that the fluid in the upper aquifer has constant density  $\rho + \Delta\rho$  and that in the lower aquifer has constant density  $\rho$ . Also we assume the resistance to flow is much greater in the fractures than the aquifer, so that the pressures in the upper and lower aquifers are each approximately uniform (see below). In this case, if the pressure in the lower layer,  $p_l$ , exceeds the hydrostatic pressure of the light fluid in the fracture plus the pressure of the upper layer,  $p_u$ , by an amount  $\Delta p$  where  $0 < \Delta p < \Delta\rho gh$  so that  $p_l = (p_u + \rho gh) + \Delta p$  then downflow or upflow can occur in the different fractures since the pressure in the lower layer is not sufficient to balance a fracture full of the dense upper layer fluid, but is more than sufficient to balance a fracture full of the light lower layer fluid. Without loss of generality, we label the fractures with downflow ( $d$ ) as  $i = 1, \dots, n$  and those with upflow ( $u$ ) as  $i = n + 1, \dots, m$ . The total downflow and upflow volume fluxes per unit length along the fractures are then given by

$$Q_d = \frac{(\Delta\rho gh - \Delta p)}{\mu h} \sum_{i=1}^n k_i d_i, \quad (2.1)$$

$$Q_u = \frac{(\Delta p)}{\mu h} \sum_{i=n+1}^m k_i d_i, \quad (2.2)$$

where we assume the fractures with upward flow are entirely filled with the less-dense lower aquifer fluid and those with downward flow are filled with the more-dense,  $\text{CO}_2$ -saturated fluid. In figure 2(a), we illustrate the magnitude of the upflow volume flux, per unit length of fracture, for the case of a 10-fracture system, showing the

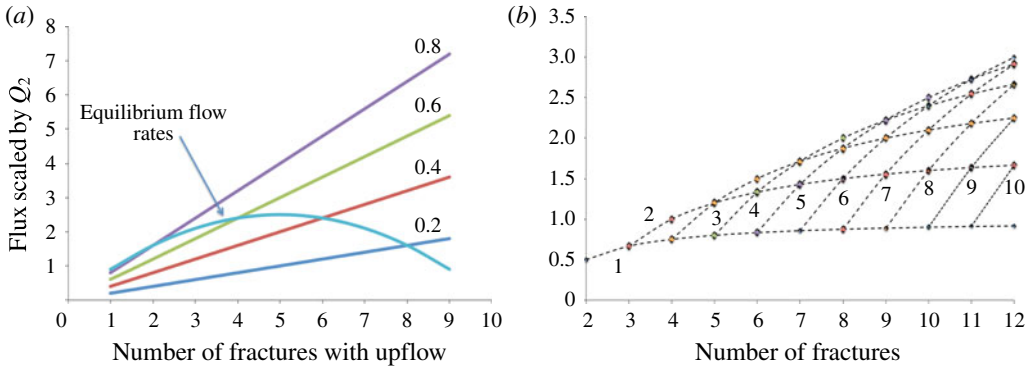


FIGURE 2. (Colour online) (a) Model predictions of the exchange flow, scaled by the buoyancy-driven flow  $Q_2$  (2.3), as a function of the number of fractures in which there is upflow in the case that there are 10 fractures in total connecting the aquifers. Curves are given for four values of the pressure difference between the aquifers, scaled relative to  $\Delta\rho gh$ . The curved line denotes the equilibrium solution in which there is no net flux of fluid between the aquifers. (b) Model predictions of the total upflow, scaled relative to  $Q_2$  (2.3), in the case of no net flux, as a function of the number of fractures connecting the upper and lower aquifers. The symbols denote the different possible equilibrium solutions. The dashed lines connect those solutions for which the number of fractures with upflow is constant, as shown on each line. The non-uniqueness in flow regime associated with different initial conditions can lead to ambiguity in model predictions.

flow as a function of the number of fractures which involve upflow. For simplicity we have assumed that the aperture,  $d_i$ , and permeability,  $k_i$ , of each fracture have the same value,  $d$  and  $k$ . Curves are shown for several different values of the pressure difference between the lower and the upper aquifer, expressed as the dimensionless fraction  $\Delta p/\Delta\rho gh$ . The volume flux, per unit length of fracture, is normalised by the value  $Q_2$  where

$$Q_2 = \frac{k\Delta\rho gd}{\mu}. \tag{2.3}$$

As expected, it is seen that as the pressure difference between the two layers increases, or the number of upflowing fractures increases, with a fixed total number of fractures, the upward flux also increases, with a corresponding decrease in the downward flux. On the figure we have also illustrated the flux which arises in the case that the upflow volume flux matches the downflow volume flux, as shown by the curved line. In this special case there is no net volume flux; this leads to the expression for the volume flux per unit length along the fracture

$$Q = \frac{\Delta\rho g}{\mu} \left( \frac{1}{\sum_1^n k_i d_i} + \frac{1}{\sum_{n+1}^m k_i d_i} \right)^{-1}. \tag{2.4}$$

The total flux in the upflowing fractures for this equilibrium exchange flow depends nonlinearly on the number of fractures in which there is upflow, since the pressure

difference between the two aquifers takes on a different value for each case. This may be seen by the intersection of the curved line with the straight lines, each of which corresponds to a constant pressure difference between the lower and upper aquifer. The actual flow which develops in practice depends on the initial conditions in the individual fractures and aquifers; there may be a range of transient flow patterns as the system adjusts to equilibrium from the different possible initial conditions, but this is beyond the scope of the present work in which our main purpose is to establish the non-uniqueness of the convective exchange.

In the non-equilibrium solutions presented above, (2.1)–(2.2), the flow in each fracture is assumed unidirectional (for  $m > 1$ ), and the net flux between the aquifers is such that the aquifer to which there is a greater volume flux will gradually increase in pressure, while the other aquifer will gradually decrease in pressure, so that the system adjusts to the equilibrium situation in which there is no net flux between the aquifers. If the pressure difference between the aquifers changes slowly, then the flow rate in each fracture also changes slowly, but the direction of flow does not change. In order to arrest the upflow in any upflowing fracture, the pressure difference between the two aquifers would need to be balanced by a partial flooding of the fracture with the heavier fluid from above, to a depth  $h_f$ , so that  $\Delta\rho gh_f = \Delta p$ ; similarly, in order to reverse the flow in an upflow fracture, the fracture would need to be flooded with light fluid from below to the depth  $h - h_f$ . As seen in figure 2, there is a range of equilibrium flow regimes across the whole interval  $0 < \Delta p / \Delta\rho gh < 1.0$  and so in general a finite depth of a given fracture would need to be flooded with the other fluid in order to reverse the flow.

It is implicit in this model that, over the inter-fracture distance, there is only a small lateral pressure change in the upper and lower aquifers, relative to the pressure change between the aquifers, so that we can take the aquifer pressure to be approximately uniform. If the fractures are a distance  $L$  apart, and the flux in a given fracture is  $\alpha Q_2$  where  $\alpha$  is of order 1, then the pressure change over the inter-fracture distance  $L$  in the upper and lower aquifers, of permeability  $K_1$ ,  $K_2$  and thickness  $H_1$  and  $H_2$ , scales as

$$\Delta p_a = \alpha Q_2 \frac{L\mu}{H_i K_i}. \quad (2.5)$$

This is small compared to the pressure difference between the aquifers, provided the ratio

$$R = \frac{k_i d_i L}{K_i H_i h} \quad (2.6)$$

of the net vertical conductivity of the fractures to the horizontal conductivity of the aquifer,  $H_i K_i$ , times the ratio  $L/h$  of the inter-fracture distance to the vertical distance between the aquifers, is small. This will typically be the case with narrow fractures, with relatively thick or highly permeable aquifers, or with a relatively thick layer of impermeable seal rock,  $h$ .

We now explore these equilibrium solutions, in which there is no net mass flux, in more detail. When there are two equal fractures, one involves upflow and one downflow, and the total volume flux per unit length in each fracture has value  $Q_2/2$ . With additional equal fractures, the total flux in the upflowing fractures increases, but depends on whether the additional fractures involve up- or downflow. For example, with  $2n$  fractures, the total flux of the upflowing fractures ranges from a lower bound of  $(2n - 1)Q_2/2n$ , which arises when all but one fracture is either upflowing or downflowing, to the upper bound of  $nQ_2/2$ , when there are  $n$  upflowing and  $n$



downflowing fractures (cf. (2.3)). In figure 2(b) we illustrate how the total upflow flux varies depending on the total number of fractures and the number of these fractures in which there is upflow, assuming that each fracture has the same aperture width and permeability. It is important to recognise that, for a given total number of fractures, each of the equilibrium solutions corresponds to a different equilibrium pressure difference between the two aquifers, as may be seen in the particular case of 10 fractures shown in figure 2(a). With non-uniform values for the aperture width and permeability of each of the fractures, as would be the case in a real geological system, there may be a broader range of flow rates, again depending on which fractures involve up- or downflow; the model may be applied in that case by specifying the direction of flow of each fracture in turn, and then determining the pressure difference between the layers so that the overall flux is zero.

In the limit of a single fracture of aperture width  $d$ , lateral extent  $L \gg d$  and permeability  $k$ , one may envisage that the upflow region occupies a fraction  $\kappa$  in the along-fracture direction, with speed  $u_u$ , and the downflow fills the remaining fraction  $1 - \kappa$  of the fracture, with speed  $u_d$ . In the case that there is no net volume flux, we require

$$\kappa u_u = (1 - \kappa) u_d \quad (2.7)$$

and the net upward (downward) volume flux, in the upflow (downflow) region, has value

$$Q = \frac{k \Delta \rho g}{\mu} \alpha (1 - \kappa) d L. \quad (2.8)$$

With this flow, there is an interface between the upflowing and downflowing regions, and CO<sub>2</sub> may diffuse across this zone. As a simple estimate, the diffusion thickness may scale as  $d_m \sim (DT)^{1/2}$  where the travel time from the lower to the upper boundary is given by  $T \sim HdL/Q$ , and where  $D$  is the diffusivity (Phillips 1991), leading to a diffusive mixed region of width

$$d_m \sim \left[ \frac{D \mu H}{k g \Delta \rho} \right]^{1/2}. \quad (2.9)$$

For typical properties, with  $D \sim 10^{-9} \text{ m}^2 \text{ s}^{-1}$ , viscosity  $\mu \sim 10^{-3} \text{ Pa s}^{-1}$ , density difference  $\Delta \rho \sim 10 \text{ kg m}^{-3}$ , and permeability  $k \sim 10^{-12} - 10^{-14} \text{ m}^2$  we find that the thickness of this diffusive layer may be of order 1–10 m. With a fracture or permeable layer extending a distance of 100–1000 m laterally, this diffusive zone is relatively small, and so (2.8) provides a good leading-order estimate for the flux. Again, the initial and boundary conditions determine the value of  $\kappa$  which develops in practice; the upflow flux has a maximum when  $\kappa = 0.5$ , but assuming all values of  $\kappa$  ( $0 < \kappa < 1$ ) are equally likely, we find that the mean value of the flux is 1/3 of the maximum flux. The single fracture problem is analogous to the continuum limit of the many fracture problem considered above, if  $\kappa$  is interpreted as the fraction of the total number of fractures involving upflow. It follows that if all distributions of upflow and downflow are equally likely, then the expected total upflow flux with  $2n$  fractures will have value  $nQ_2/6$ . Note that in the case of a single fracture, there is an unstable equilibrium in which the upper part of the fracture is filled to a uniform depth with dense upper aquifer fluid, and the lower part filled with the less-dense lower aquifer fluid, to exactly compensate for the pressure difference between the layers: however, this situation is unstable to convective overturn within the fracture leading to the single fracture exchange flow described above.

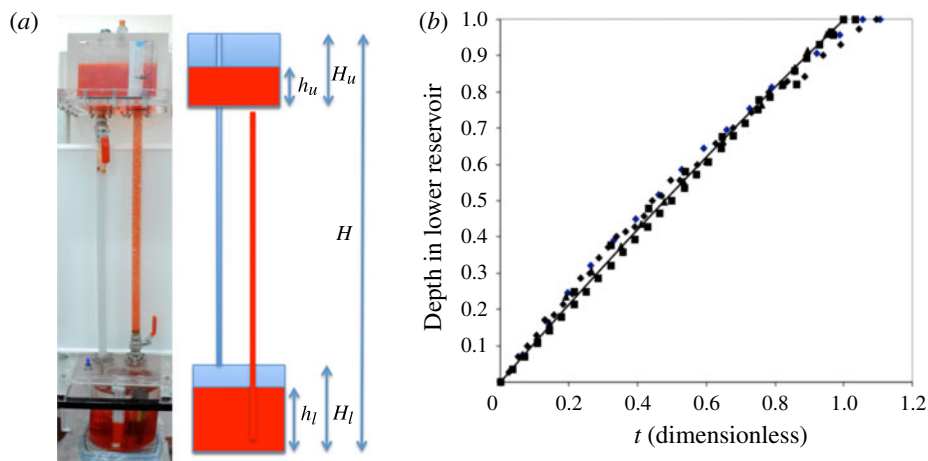


FIGURE 3. (Colour online) (a) Photograph and schematic of the experimental system to model a two-tube exchange flow. The darker grey (red online) fluid is saline, and lighter grey fluid is fresh; and the vertical tubes separating the two reservoirs are filled with 1 mm glass ballotini to produce a model of a permeable fracture. (b) Experimental results showing the depth of the saline layer in the lower reservoir,  $h_l/H_l$ , as a function of dimensionless time as measured in a series of different experiments using different values of the salinity of the descending fluid, 1.5, 3.7, 6, 6 and 14 wt%. In each case the ascending fluid is fresh. The dimensionless time is defined by (3.3).

### 3. Experimental modelling

We have tested the above model with a simple analogue laboratory experiment of exchange flows between aquifers. The experimental system consists of two vertical tubes, of diameter 2 cm and length 1 m, each filled with glass ballotini as a model of the fractures. The tubes are connected to an overlying sealed reservoir initially filled with aqueous saline solution, and the lower ends of the tubes are immersed in a second reservoir, initially filled with fresh water (figure 3a).

The fresh-water reservoir is placed on a mass balance to record changes in the mass with time. One tube is initially filled with fresh water, and the top of this tube is located near the top of the upper reservoir, so as to minimise the mixing of the ascending fresh water with the fluid in the top reservoir tank. Similarly, the other tube is initially filled with saline solution, and this opens near the base of the lower tank, so as to limit mixing with the fresh water. The exchange flow commences by opening a valve in each tube, and subsequently a layer of fresh water accumulates in the top of the upper reservoir, and a layer of saline solution in the base of the lower reservoir. This initial set-up of the experiment may be different from the case in which the target aquifer is overpressured during injection and from which fractures then develop and grow. However, if there are some pre-existing fractures which fail during the injection process, one may envisage that these extend independently from either the upper or lower aquifer and hence may initially be filled with either upper or lower layer fluid; nonetheless, our experiments are designed to illustrate the exchange flow phenomena and, given the geological uncertainties, we do not model the complexity of the fracturing which leads to the specific initial conditions.

A series of experiments were conducted with salt concentrations in the upper reservoir taking the values 1.5, 3.7, 6, 6 and 14 wt%, and the rate of change of the



mass of the lower tank, and the depth of the fresh water layer in the upper tank were measured as a function of time. The upflow pipe draws fluid from the top of the lower reservoir and extends to the top of the upper reservoir, producing a layer of fresh water of depth  $h_u(t)$  at the top of the upper reservoir, of total depth  $H_u$ , while the downflow pipe draws fluid from the base of the upper reservoir and extends to the base of the lower reservoir, producing a layer of saline water of depth  $h_l(t)$  at the base of the lower reservoir which has total depth  $H_l$ . The buoyancy derived difference in the pressure across the upflow and downflow pipe is given by  $\Delta\rho g(H - h_u - h_l)$ , where  $H$  is the distance from the top of the upper tank to the base of the lower tank (figure 3a). This pressure is dissipated over a length  $H - H_u$  for the downflow pipe and a length  $H - H_l$  for the upflow pipe. Using the results from the previous section, we infer that the flux of fresh water entering the upper reservoir, and saline water entering the lower reservoir is

$$Q = \left( \frac{k_p \Delta\rho g A_p}{\mu} \right) \frac{(H - h_u - h_l)}{(2H - H_u - H_l)}. \quad (3.1)$$

This leads to a deepening of the saline water layer, of depth  $h_l(t)$ , in the lower reservoir tank, of cross-sectional area  $A_l$  according to the relation

$$\frac{d\left(\frac{h_l}{H_l}\right)}{d\tau} = \frac{H - h_u - h_l}{2H - H_u - H_l}, \quad (3.2)$$

where the scaled time is given by

$$t = \left( \frac{\mu A_l H_l}{k_p \Delta\rho g A_p} \right) \tau, \quad (3.3)$$

with  $k_p$  and  $A_p$  the permeability and cross-sectional area of the porous upflow and downflow pipes. We have plotted our experimental measurements of  $h_l/H_l$  as a function of time in dimensionless form, as given by (3.3), in figure 3(b), where it is seen there is good agreement with the model. In calculating the scaled time we used a value for the permeability of the ballotini-packed vertical columns as measured from an independent experiment.

In order to demonstrate that the system has multiple flow solutions, we have also built a tank with five vertical pipes representing five fractures, connecting an upper and a lower reservoir. When the upper and lower reservoirs are filled with saline solution and fresh water, an exchange flow develops, with upflow in some pipes, and downflow in others. The direction of flow depends on the initial fluid density in each of the pipes; by filling some with fresh and some with saline fluid, the system can be driven into each of the different flow regimes. Figure 4 illustrates an example in which pipes 3 and 4 involve downflow from the upper reservoir, while the other three pipes, 1, 2 and 5, involve upflow from the lower reservoir. In pipe 5, a relic transient downflowing plume of darker fluid can be seen which developed in the very early stages of the experiment. Such initial transient behaviour tends to develop in the case that the pipes are filled with some upper and some lower layer fluid, so that there is an initial evolution of the flow towards a steady exchange flow regime; however, once a quasi-steady flow, with unidirectional flow in each pipe, has become set up, it tends to remain stable.

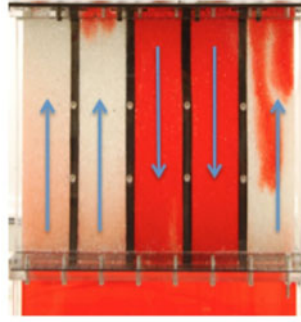


FIGURE 4. (Colour online) Illustration of a five-layer experimental system, in which there are five independent channels from the upper reservoir, originally containing darker grey (red online) saline fluid, to the lower reservoir, originally containing clear fresh lighter grey fluid; each channel represents an analogue of a fracture. In the experiment shown, there is downflow in two of the channels and upflow in three of the channels. In the right-most channel, a relic streak of darker grey fluid may be seen; this is associated with a transient descending parcel of saline fluid during the initial stages of the flow, before a steady upflow in this channel was established.

#### 4. Implications

This model allows us to estimate the flux of unsaturated water which may be carried to the  $\text{CO}_2$ -water interface and drive dissolution if there are fractures in a layered sedimentary formation which connect a deep aquifer with a shallow aquifer containing a trapped pocket of  $\text{CO}_2$  (figure 1*b*). In the upper aquifer, in contact with the trapped pocket of  $\text{CO}_2$ , convective mixing will lead to near  $\text{CO}_2$ -saturation conditions in the water driven by the convection in the upper layer (figure 1*a*) (Hewitt *et al.* 2013).

If the anticline structure is dominantly two-dimensional, perhaps aligned with the faults, and the  $\text{CO}_2$  plume extends a distance  $L$  in the cross-anticline direction (figure 1*b*), then the nearly horizontal convective exchange flow between the  $\text{CO}_2$ -saturated fluid below the trapped  $\text{CO}_2$  plume and the more distal unsaturated fluid in the upper aquifer, of permeability  $K_1$  and thickness  $H_u$ , has a maximum value per unit length given by (Woods & Espie 2012)

$$F_l \sim \frac{K_1 \Delta \rho g}{2\mu} H_u \sin \theta, \quad (4.1)$$

where the inclination of the aquifer to the horizontal is  $\theta$ . With  $2n$  fractures, each of aperture width  $d$ , over the lateral extent of the  $\text{CO}_2$  plume,  $L$ , then, according to the model herein, we expect the volume flux between the upper aquifer and the lower aquifer, driven by the relatively dense  $\text{CO}_2$ -saturated water to be of order

$$F_f = \frac{k \Delta \rho g}{6\mu} n d. \quad (4.2)$$

In the limit that

$$k n d \gg K_1 H \sin \theta \quad (4.3)$$

the vertical exchange flow through the fractures from the deeper aquifer to the upper layer will dominate the lateral exchange flow in the upper aquifer in driving continued

dissolution of the CO<sub>2</sub> plume, once the fluid immediately below the trapped plume has become saturated. In natural systems, there are many possible parameter values, but with sufficiently permeable or densely spaced fractures, this is a realistic limit. For example, even if the cumulative aperture widths of the fractures over the width of the trapped plume of CO<sub>2</sub> only occupy 10–100 cm, this may represent 1%–10% of the thickness of the upper aquifer. With a shallow incline,  $\sin \theta = 0.1$ – $0.01$ , and with fractures which are 100 times more permeable than the formation, the resupply of unsaturated water to drive dissolution may then be dominated by the exchange flow from the lower aquifer. Note that the volume flux of convective plumes of fresh water rising through the upper layer from a distributed source of lateral extent  $L$  would scale as  $LK_1\Delta\rho g/\mu$ ; this is much greater than the flux of unsaturated fluid supplied by the fractures provided  $LK_1 \gg knd$ , as would typically be the case for a shallow anticline. It follows that the fluid supplied by the fractures becomes rapidly mixed through the upper aquifer.

## 5. Discussion

We have demonstrated the potential for buoyancy differences to drive exchange flows along fractures through the seal rock between aquifers. Such exchange flows may be important in quantifying the time-history of dissolution of a trapped plume of CO<sub>2</sub> during carbon sequestration. Our modelling has shown that significant buoyancy-driven exchange flows may develop which may control the supply of unsaturated water driving dissolution of the CO<sub>2</sub> once the fluid directly below the CO<sub>2</sub> plume has become CO<sub>2</sub> saturated. In equilibrium, such exchange flows may not lead to any net transport of fluids, but can lead to substantial spreading of contaminated fluid from one layer to another within the subsurface over long time scales if there are buoyancy contrasts between aquifers. This may represent an important buoyancy-driven dispersion process over long time scales (Croucher & O'Sullivan 1995; Levy & Berkowitz 2003; Flowers & Hunt 2007), with important consequences on risk assessments for geological storage systems. Finally, we note that the non-uniqueness of the flow regime can lead to a wide range of fluid exchange rates depending on the initial conditions of the system; such non-uniqueness adds uncertainty to our predictions of the time scales required for dissolution of injected CO<sub>2</sub>. In our models we have assumed that in a multi-fracture system, there is unidirectional flow in each fracture, as also observed in steady state in our experiments; in practice, it may be that with certain initial conditions, counterflows may also develop within individual fractures, as well as there being differences in the flow between fractures, and it may be interesting to explore such additional complexity in a further study.

In closing we note that in some natural situations in geological strata with two different permeable aquifers, there may be a temperature contrast as well as salinity contrast between the fluids in the two aquifers. This can lead to a further class of interesting exchange flow problems, related to the double-advective instability (Phillips 1991; Woods 2015). This instability arises owing to the thermal inertia which causes the fluid near the leading edge of an advancing front to acquire the local temperature of the formation (e.g. Menand, Raw & Woods 2003). Consider the case in which a hot but weakly saline fluid, fluid A, in one aquifer is connected by a series of fractures to a cold but relatively fresh fluid, fluid B, in the other aquifer, and in which the temperature contrast dominates salinity contrast in controlling the density difference. Then, for example, the system may be statically stable if the hot saline

fluid (fluid A) is in the upper aquifer. However, if some upper layer fluid flows down a fracture, it will cool and become relatively dense compared to the lower layer fluid (fluid B), owing to its greater salinity, leading to continued descent. Similarly, if some lower layer cold but fresh fluid rises up a fracture, it will heat up, while remaining fresh, and so will become buoyant relative to the upper layer fluid and continue to ascend. As a result, there may be instability and a convective exchange between the two aquifers even though they are statically stable. In contrast, if the relatively saline and hot fluid A is in the lower aquifer, with the denser, cold but relatively fresh fluid B in the upper aquifer, then this can lead to a statically unstable situation. However, the system may be dynamically stable, since the hot saline fluid will rise and cool, thereby becoming dense and falling back into the lower layer, suppressing the exchange flow. The dynamics of such a system have been simulated and analysed by Oldenburg & Rinaldi (2011). Although this flow regime is more complex, owing to both the thermal and salinity fields, in the case that the system is dynamically unstable, the non-uniqueness of the exchange flow pattern that develops will be analogous to the non-uniqueness that we observe in this work, again leading to a non-unique flux.

## REFERENCES

- BEAR, J. 1981 *Introduction to Flow in Porous Media*. Wiley.
- BENNION, B. & BACHU, S. 2008 Drainage and imbibition relative permeability relationships for supercritical CO<sub>2</sub>/Brine and H<sub>2</sub>S/Brine systems in intergranular sandstone, carbonate, shale and anhydrite rocks. *SPE Reservoir Eval. Engng* **11** (3), 487–496.
- CHEN, C. & ZHANG, D. 2010 Pore-scale simulation of density-driven convection in fractured porous media during geological CO<sub>2</sub> sequestration. *Water Resour. Res.* **46**, W11527.
- CROUCHER, A. E. & O'SULLIVAN, M. J. 1995 The Henry problem of salt–water intrusion. *Water Resour. Res.* **31**, 1809–1814.
- DIERSCH, H.-J. & KOLDITZ, O. 2002 Variable-density flow and transport in porous media: approaches and challenges. *Adv. Water Resour.* **25**, 899–944.
- ENNIS-KING, J. & PATERSON, L. 2007 Coupling of geochemical reactions and convective mixing in the long-term geological storage of carbon dioxide. *Intl J. Greenh. Gas Control* **1**, 86–93.
- FARCAS, A. & WOODS, A. W. 2009 The effect of drainage on the capillary retention of CO<sub>2</sub> in a layered permeable rock. *J. Fluid Mech.* **618**, 349–359.
- FLOWERS, T. & HUNT, J. 2007 Viscous and gravitational contributions to mixing during vertical brine transport in water-saturated porous media. *Water Resour. Res.* **43**, WR004773.
- FRIED, J. J. & COMBARNOUS, M. A. 1971 Dispersion in porous media. *Adv. Hydrosci.* **7**, 169–282.
- GREEN, C. P. & ENNIS-KING, K. 2010 Effect of vertical heterogeneity on long-term migration of CO<sub>2</sub> in saline formations. *Transp. Porous Med.* **82**, 31–47.
- HESSE, M., TCHHELPI, M. & ORR, L. 2008 Gravity currents with residual trapping. *J. Fluid Mech.* **611**, 35–60.
- HEWITT, D., NEUFELD, J. & LISTER, J. 2013 Convective shutdown in a porous medium at high Rayleigh number. *J. Fluid Mech.* **719**, 551–586.
- INTERGOVERNMENTAL PANEL ON CLIMATE CHANGE 2005 *IPCC Special Report on Carbon Dioxide Capture and Storage*. Cambridge University Press.
- KUZNETSOV, A. V. & NIELD, D. A. 2011 The effects of combined horizontal and vertical heterogeneity on the onset of convection in a porous medium with vertical throughflow. *Transp. Porous Med.* **90**, 465–478.
- KUZNETSOV, A. & NIELD, D. A. 2012 The effect of strong heterogeneity and strong throughflow on the onset of convection in a porous medium: periodic and localized variation. *Transp. Porous Med.* **92**, 289–298.

- LEVY, M. & BERKOWITZ, B. 2003 Measurement and analysis of non-Fickian dispersion in heterogeneous porous media. *J. Contam. Hydrol.* **64** (3–4), 203–226.
- LINDBERG, E. & WESSEL-BERG, D. 1997 Vertical convection in an aquifer column under a gas cap of CO<sub>2</sub>. *Energy Convers. Manage.* **38**, S229–S234.
- MENAND, T., RAW, A. & WOODS, A. W. 2003 Thermal inertia and reversing buoyancy in flow in porous media. *Geophys. Res. Lett.* **30** (6), 1241–1245.
- OLDENBURG, C. M. & RINALDI, A. P. 2011 Buoyancy effects on upward brine displacement caused by CO<sub>2</sub> injection. *Transp. Porous Med.* **87** (2), 525–540.
- PAU, G., BELL, J. B., PRUESS, K., ALMGREN, A. & LIJENSKI, M. 2009 High resolution simulation and characterisation of density driven flow in CO<sub>2</sub> storage in saline aquifers. *Adv. Water Resour.* **33**, 443–455.
- PHILLIPS, O. M. 1991 *Flow and Reaction in Permeable Rocks*. Cambridge University Press.
- PRUESS, K., XU, T., APPS, J. & GARCÍA, J. 2003 Numerical modeling of aquifer disposal of CO<sub>2</sub>. *SPE J.* **8**, 49–60.
- RANGANATHAN, P., FARAJZADEH, R., BRUINING, H. & ZITHA, P. 2012 Numerical simulation of natural convection in heterogeneous porous media for CO<sub>2</sub> geological storage. *Trans. Porous Med.* **95**, 25–54.
- RIAZ, A., HESSE, M., TCHELEPI, H. A. & ORR, F. M. JR 2006 Onset of convection in a gravitationally unstable diffusive boundary layer in porous media. *J. Fluid Mech.* **548**, 87–111.
- SCHEIDEGGER, A. E. 1961 General theory of dispersion in porous media. *J. Geophys. Res.* **66**, 3273–3274.
- SZULCZEWSKI, M. L., HESSE, M. A. & JUANES, R. 2014 Carbon dioxide dissolution in structural and stratigraphic traps. *J. Fluid Mech.* **736**, 287–315.
- TARTAKOVSKY, A. & MEAKIN, P. 2005 A smoothed particle hydrodynamics model for miscible flow in three-dimensional fractures and the two-dimensional Rayleigh–Taylor instability. *J. Comput. Phys.* **207**, 610–624.
- WOODS, A. W. 2015 *Flow in Porous Rocks*. pp. 1–289. Cambridge University Press.
- WOODS, A. W. & ESPIE, A. 2012 Controls on the dissolution of CO<sub>2</sub> plumes in structural traps in deep saline aquifers. *Geophys. Res. Lett.* **39**, L08401.